Journal of Nano- and Electronic Physics
Vol. **18** No 1, 01030(9pp) (2026)

Журнал нано- та електронної фізики
Том **18** № 1, 01030(9cc) (2026)

OPEN ACCESS

REGULAR ARTICLE

Study of Pore Distribution in Activated Carbon by Low-Temperature Nitrogen Adsorption

V.M. Vashchynskyi* ✉, Ya.B. Vashchynska

Lviv Polytechnic National University, 79013 Lviv, Ukraine

(Received 30 October 2025; revised manuscript received 18 February 2026; published online 25 February 2026)

Activated carbon (AC) samples were prepared from apricot kernel shells waste using a two-step pyrolytic activation process. The influence of carbonization temperature on the pore structure and pore size distribution of the ACs was investigated. The results showed that a high activation temperature and chemical activation with potassium hydroxide (KOH) promote the development of porosity. In this study, the pore structure was analyzed by nitrogen adsorption–desorption measurements at 77 K over a wide relative pressure range ($P/P_0 = 0.050 – 1.0$). Carbonization of apricot kernel shells at 300°C accelerates the removal of volatile components and leads to the formation of a larger number of mesopores, whereas increasing the temperature to 400 – 600°C favors the development of a microporous structure. The highest specific surface area, determined by the Brunauer–Emmett–Teller (BET) method, was obtained for sample AC31 and amounted to 1313 $m^2 g^{-1}$, while the pore diameter determined by the Barrett–Joyner–Halenda (BJH) method was 2.25 nm. The V_{micro} values obtained for all synthesized AC samples correlate well with those determined by the Horvath–Kawazoe (HK) and Saito–Foley (SF) methods, which take into account the contribution of narrow cylindrical pores. According to the t-plot method, the largest micropore volume was 0.469 $cm^3 g^{-1}$ for sample AC61 carbonized at 600°C.

Keywords: Apricot kernel shells, Carbonization temperature, Activated carbon, Adsorption Isotherm, Pore structure.

DOI: 10.21272/jnep.18(1).01030 PACS numbers: 81.05.Rm, 68.43. – h, 61.46. + w

1. INTRODUCTION

At present, the study of the structure of activated carbon (AC) is of significant scientific and practical interest, since the range of applications of these materials continues to expand, including electronics, metallurgy, electrochemistry, membrane and sorption technologies for water and soil purification, aerospace technologies, and nuclear energy. The wide spectrum of AC applications is justified by the diversity of carbon precursors, which leads to different physical and chemical properties. One of the distinctive features of ACs derived from plant biomass is that they can be produced under various pyrolysis and activation conditions using an extremely broad range of precursors. The diversity of their final properties can be achieved through specific physicochemical treatments of carbon-containing precursors. Traditionally, activated carbon is obtained by carbonizing raw materials of plant origin, such as hardwood, fruit stones, nutshells, husks, or cellulose (Fig. 1). At this stage, volatile compounds are released, resulting in the removal of moisture and, partially, pyrolytic tar [1]. However, carbonized materials derived from fruit stones usually exhibit low porosity, and their structure is characterized by numerous small pores filled with pyrolysis products [2, 3]. The task of obtaining a specific microporous structure is accomplished during the activation process. During activation, closed pores are opened and a porous structure is formed. Activation can be carried out by two main methods: oxidation with gas or steam at 800–1000°C (physical activation), or by chemical treatment of the carbonaceous precursor with activating agents such as phosphoric, sulfuric, or nitric acids, as well as nitrates or sulfates, at 200 – 650°C. The final properties AC – such as highly developed porosity and high carbon content – depend on the type of precursor and the synthesis conditions. For instance, AC obtained from nutshells using a mixture of physical activating agents (CO_2 and steam) exhibits high mechanical strength [4], whereas activated carbon produced via chemical activation of fruit and olive stones [5] is characterized by a well-developed mesoporous surface [6].

By varying the activation temperature, duration, and type of activating agent, it is possible to control the total pore volume, specific surface area, and pore size distribution. Gas adsorption plays a crucial role in characterizing a wide range of porous materials. Among the various gases and vapors commonly used as adsorbates, nitrogen remains the universal standard. The surface area and pore size distribution of solid catalytic materials can be determined through gas adsorption–desorption measurements at 77 K.

* Correspondence e-mail: v.vashchynskyi@gmail.com

Cite this article as: V.M. Vashchynskyi et al., *J. Nano- Electron. Phys.* 18 No 1, 01030 (2026) https://doi.org/10.21272/jnep.18(1).01030

Fig. 1 – Schematic representation of the porous structure of activated carbon derived from biowaste

For accurate pore structure analysis, nitrogen adsorption–desorption isotherms should be measured over the widest possible range of relative pressures, taking into account the slow equilibration and other operational challenges, particularly at very low pressures. Numerous methods exist for calculating surface area, pore size, pore volume, and pore size distribution by fitting isotherm data to different models. For example, the Brunauer–Emmett–Teller (BET) method is typically employed to determine the specific surface area, whereas the Barrett–Joyner–Halenda (BJH) model [7] is used to analyze pore size distribution based on the corresponding isotherm. Singh et al. classified pores in the context of physical adsorption into four categories according to their size: macropores (>50 nm), mesopores (2 – 50 nm), micropores (< 2 nm), and ultramicropores (< 0.7 nm) [8]. It should be noted that the gas adsorption mechanism differs substantially depending on the average pore diameter of the material. Dubinin proposed that very narrow pores (micropores up to 2 nm wide) become filled at low relative pressures through a volume filling process [9]. This micropore filling mechanism differs fundamentally from the capillary condensation process occurring in mesopores [8]. All the above-mentioned findings and experimental data are of great importance and serve as a fundamental basis for the synthesis of new high-porosity materials with tailored properties. Considering recent advances in computational modeling of surface morphology and the application of density functional theory (DFT) to describe the properties of carbon materials [10], the aim of this study is to investigate the porous structure of activated carbons using a comprehensive set of porometric analysis methods (BET, BJH, DFT, and the *t*-method).

2. MATERIALS AND METHODS

2.1 Synthesis of Activated Carbon

In our view, the production of activated carbons (ACs) from plant biomass represents the most relevant and sustainable approach due to the low cost, environmental friendliness, and wide availability of natural precursors. In this study, activated carbon was synthesized from apricot shell biomass through a two-step process involving carbonization followed by chemical activation using potassium hydroxide (KOH). In the first stage, dried apricot kernel shells were separated from their kernels, and the shells were crushed to a particle size fraction of 0.25 – 1 mm. The raw material was then carbonized at temperatures ranging from 300 to 900°C with an increment of 100°C at a heating rate of 10°C min^{-1}. After cooling, the carbonized material was mechanically ground to a particle size of 200 – 250 μm and mixed with potassium hydroxide and deionized water in a weight ratio W_R = 1:1, where W_R = m(KOH)/m(C).

The resulting mixture was thoroughly stirred for 1 – 2 h, followed by drying in a thermostat at 90°C to a constant weight. The dried material was then placed in a tubular furnace and heated in an argon atmosphere at 900 – 920°C with a heating rate of 10°C min^{-1}, maintaining this temperature for 20 min. The obtained carbonaceous product was washed sequentially with hydrochloric acid and deionized water until a neutral *pH* was reached to remove mineral impurities and ash, and then dried to constant weight in a drying oven. The prepared carbon samples were designated as ACxy, where x = 3, 4, 5, 6, 7, 8, 9 corresponds to the carbonization temperature (in hundreds of °C), and y = 1 indicates the KOH-to-carbon weight ratio. For example, AC51 refers to the sample carbonized at 500°C and activated with an equal mass ratio of KOH to carbon. Accordingly, a series of samples designated as AC31 – AC91 was obtained.

2.2 Characterization Methods

The textural characteristics of the activated carbon (AC) samples were determined based on the analysis of nitrogen adsorption–desorption isotherms measured at the boiling temperature of liquid nitrogen (77 K) using a NOVA 2200e surface area and porosity analyzer (Quantachrome Instruments, USA). Prior to the measurements, all samples were degassed under vacuum at 180 °C for 18 h remove adsorbed moisture and volatile impurities. The specific surface area (S_{BET}, $\text{m}^2 \cdot \text{g}^{-1}$) was calculated by the multipoint Brunauer–Emmett–Teller (BET) method in the relative pressure range P/P_0 = 0.05–0.35 of the adsorption isotherm. The total pore volume (V_{total}, $\text{cm}^3 \cdot \text{g}^{-1}$) was evaluated from the amount of nitrogen adsorbed at $P/P_0 \approx 1.0$. The micropore volume (V_{micro}, $\text{cm}^3 \cdot \text{g}^{-1}$) as well as the specific surface areas of micro- and mesopores (S_{micro}, S_{mezo}, $\text{m}^2 \cdot \text{g}^{-1}$) were determined using the *t*-plot method and Density Functional Theory (DFT) calculations [11, 12]. All textural parameters were obtained from nitrogen adsorption–desorption measurements performed on independently prepared samples. The reproducibility of BET surface area and pore volume values was within ±5%, confirming the reliability of the experimental results.

3. RESULTS AND DISCUSSION

3.1 BET Surface Area Determination

During physical adsorption, which is governed by van der Waals forces, a monomolecular layer of gas molecules is formed on the surface of activated carbon as a result of interactions between adsorbate molecules and solid surface atoms [13]. If the area occupied by a single molecule is known, the total surface area of the material can be estimated by measuring the mass of the adsorbed gas. In practice, however, the volume of adsorbed gas depends strongly on the system pressure and may significantly exceed the monolayer capacity.

Brunauer, Emmett, and Teller developed the theory of polymolecular adsorption, which allows the analysis of various types of adsorption isotherms that describe the increase in the amount of gas adsorbed on the surface over time at a constant temperature, depending on the actual (P) and saturation pressure (P_0) of the system. The Brunauer–Emmett–Teller (BET) model is based on three key assumptions [14]:

1. The adsorbent surface is homogeneous, and all adsorption sites are energetically equivalent.
2. Adsorption occurs in layers, and all adsorbed layers beyond the first are identical.
3. The model considers only the interaction between the adsorbate and the adsorbent ("vertical" forces), neglecting the interactions between adsorbate molecules within the same layer ("horizontal" forces).

Nitrogen adsorption isotherms at 77 K obtained for AC samples carbonized at different temperatures of the precursor are shown in Fig. 2. According to the International Union of Pure and Applied Chemistry (IUPAC) classification, these adsorption isotherms correspond to Type IV, which is typical for mesoporous solids, and is associated with the complete filling of micropores by the adsorbate [15]. At low relative pressures ($P/P_0 < 0.4$), a sharp increase in the amount of adsorbed N_2 is observed, corresponding to monolayer adsorption and micropore filling [16]. For all samples, the adsorption (black) and desorption branches do not coincide, forming a hysteresis loop in the region $P/P_0 \approx 0.4$–1.0. This hysteresis arises because, during desorption, condensed molecules leave the pores at lower pressures than those at which condensation occurred during adsorption. The presence of a Type H4 hysteresis loop indicates capillary condensation within mesopores.

In particular, the adsorption isotherm of sample AC31 (Fig. 2a) demonstrates that this activated carbon possesses a well-developed porous structure with a high fraction of mesopores, as evidenced by the pronounced divergence between adsorption and desorption branches in the medium-pressure range ($0.4 < P/P_0 < 0.9$). At high relative pressures ($P/P_0 > 0.8$), the filling of larger pores and interparticle voids occurs [17]. The desorption curve (colored region) also rises, but with a slightly smaller slope, reflecting capillary condensation–evaporation processes within the meso- and macropores of the material [18].

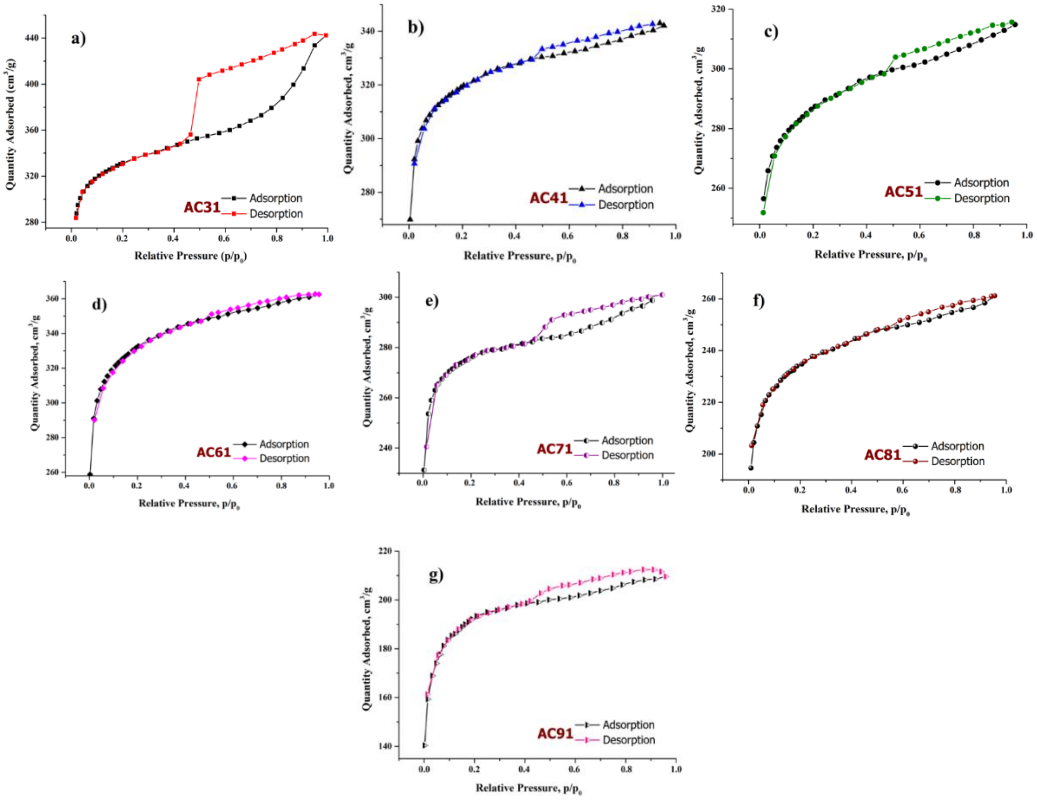

Fig. 2 – Nitrogen adsorption/desorption isotherms (77 K) of the obtained AC samples with different temperatures of carbonization: (a) 300 °C; (b) 400 °C; (c) 500 °C; (d) 600 °C; (e) 700 °C; (f) 800 °C; (g) 900 °C

The experimental data were processed using the BET equation:

$$\frac{1}{W[P/P_0-1]}=\frac{1}{W_mC}+\frac{C-1}{W_mC}(P/P_0), \quad (1)$$

where P is the equilibrium pressure of the gas, P_0 is the saturation vapor pressure, W is the mass of gas adsorbed at a given relative pressure (P/P_0), W_m is the mass of adsorbate required to form a monolayer on the entire surface of the adsorbent, and C is the BET constant, which is related to the adsorption energy of the first layer and thus characterizes the strength of the adsorbate–adsorbent interaction.

Nitrogen was used as the adsorptive gas for determining the specific surface area. For nitrogen, the C constant typically lies within the range 50–250, which prevents localized adsorption on most solid surfaces. The dependence $\frac{1}{W[P/P_0-1]}=f(P/P_0)$ has the form of a straight line with a slope $s=\frac{C-1}{W_mC}$, and an intercept $i=\frac{1}{W_mC}$ on the ordinate axis (Fig. 3) [19].

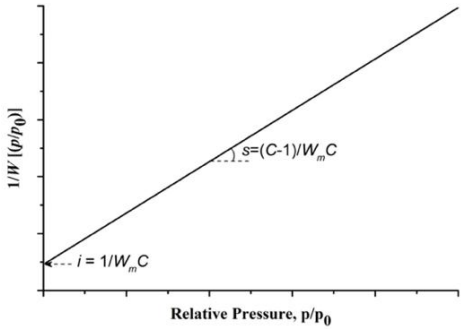

Fig. 3 – Experimental adsorption isotherm.

The obtained dependence, which determines W_m, can be used for the analysis of isotherms constructed at relative pressures P/P_0 = 0.05 – 0.35. By calculating the volume W_m of the adsorbed gas forming a monolayer, the total surface area can be determined using the equation:

$$S_t=\frac{W_m N_A A_{CS}}{M}, \quad (2)$$

where N_A is Avogadro's number, M is the molar mass of the adsorbate, and A_{CS} is the cross-sectional area of the adsorbate molecule. For a hexagonally packed monolayer of nitrogen at 77 K, the cross-sectional area of the nitrogen molecule is 0.162 nm^2.

The plots of the specific surface area determined by the BET method and the total pore volume of activated carbon obtained by thermal activation are shown in Fig. 4.

The variation in the development of the porous structure of the activated carbon at different carbonization temperatures is associated with the rapid reaction of activating agents with volatile substances that evolve, as well as with the carbon texture of the apricot kernel shells during the two-stage pyrolysis activation process [20, 21].

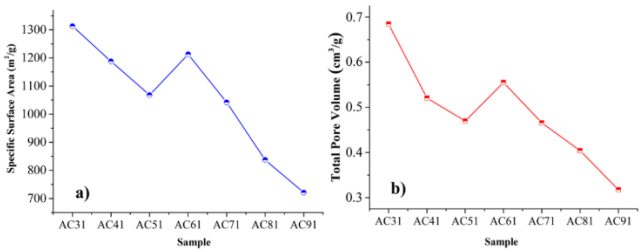

Fig. 4 – Specific surface area (a) and total pore volume (b) of activated carbon samples obtained at different carbonization temperatures

An increase in temperature from 300 °C to 500 °C results in a poorly developed porous structure, while the total pore volume decreases from 0.680 to 0.45 cm$^3\cdot$g^{-1}. Further temperature increases up to 600°C leads to an expansion of small pores, resulting in a BET surface area of 1213 m$^2\cdot$g^{-1}. A subsequent rise in the carbonization temperature from 700 °C to 900 °C causes pore sintering, which adversely affects the porosity development. Consequently, the specific surface area of sample AC91 is 48% lower than that of AC61, since substances (resins and hydrocarbons) present at high carbonization temperatures decompose and accumulate, leading to the blockage of active carbon surface sites.

3.2 Determination of Porosity

According to widely reported activation mechanisms, moderate KOH impregnation promotes the formation of a predominantly microporous structure through redox reactions, intercalation of potassium species, and subsequent gasification processes [5-6, 13]. At lower KOH contents, the activation is often insufficient, leading to limited pore opening and reduced specific surface area, whereas higher KOH-to-carbon ratios are known to intensify carbon etching, which may result in excessive pore widening, thinning of pore walls, and increased carbon burn-off. By maintaining a constant KOH-to-carbon ratio at 1:1, the present work isolates the effect of carbonization temperature on pore structure evolution, allowing a clear assessment of its role in controlling the balance between microporosity and mesoporosity. In different samples, as well as within a single sample, individual pores may vary significantly in both shape and size. In most cases, particular attention is paid to the transverse pore dimension – specifically, the diameter of cylindrical pores or the distance between the walls of slit-shaped pores [22]. The classification of pores adopted by the IUPAC states that each pore size range corresponds to characteristic adsorption properties, which are reflected in the shape of adsorption isotherms. According to this classification, micropores have sizes smaller than 2 nm, mesopores range from 2 to 50 nm, and macropores exceed 50 nm in diameter.

To determine the volume of micropores in the presence of mesopores, the Halsey t-plot method [23] is used. In this method, the nitrogen adsorption isotherm is

measured, and from it the specific surface areas of the total and microporous structures are separately determined. The t-plot represents the relationship between the volume of adsorbed gas V and the statistical thickness of the adsorbed layer t. The essence of the method [23] lies in expressing the experimental adsorption isotherm within the relative pressure range $P/P_0 = 0.20–0.50$ as a function of a new variable t, called the statistical thickness of the adsorption film, which is defined by the equation:

$$t = \sigma \frac{W}{W_m}, \quad (3)$$

where σ is the monomolecular thickness of the adsorption film, equal to 0.354 nm for nitrogen at $T = 77$ K.

Table 1 presents the comparative data on the micropore volume of activated carbons obtained at different carbonization temperatures. The results of microporous structure analysis, calculated using empirical methods, show satisfactory correlation among themselves and complement the information on total pore volume obtained from the BET method (Fig. 4). With increasing temperature, more volatile substances evaporate rapidly, leading to the formation of a greater number of porous structures within the carbon framework. These processes create efficient diffusion pathways for the release of internal volatiles, which in turn promotes the development of additional micropores [24].

Table 1 – Micropore volume values of synthesized activated carbons obtained by different methods

Sample	Volume of micropores, $cm^3 \cdot g^{-1}$			
	t-method	HK method	SF method	NLDFT method
AC31	0.438	0.504	0.507	0.641
AC41	0.416	0.438	0.440	0.450
AC51	0.403	0.428	0.430	0.437
AC61	0.469	0.489	0.491	0.505
AC71	0.398	0.423	0.424	0.428
AC81	0.330	0.354	0.356	0.374
AC91	0.273	0.291	0.292	0.303

According to the t-plot method, the maximum value of V_{micro} equals $0.469\ cm^3 \cdot g^{-1}$ for the AC61 sample carbonized at 600 °C. This result correlates well with the micropore volume determined by the Horvath–Kawazoe (HK) method, which is commonly used for evaluating the volume of narrow micropores [25]. For comparison, additional values of micropore volume for all samples were obtained using the Saito–Foley (SF) method [25] and the Non-Local Density Functional Theory (NLDFT) approach [26], considering cylindrical pore geometry. The micropore volume of seven carbon materials, determined by the NLDFT method from nitrogen adsorption isotherms and ranging from $0.303\ cm^3 \cdot g^{-1}$ to $0.641\ cm^3 \cdot g^{-1}$, is regarded as one of the most accurate approaches for analyzing porous structures, providing detailed information about the full pore size distribution.

Classical theories, such as Dubinin–Radushkevich (DR) and Dubinin–Astakhov (DA) [27], do not allow for a complete description of the filling of micropores and narrow mesopores. This leads to an underestimation of the actual pore sizes and errors in calculations. A modern approach to describing adsorption isotherms and pore size distributions for microporous materials is based on quantum-mechanical calculations, which involve constructing theoretical isotherms for various pairs of microporous adsorbents–adsorbate. These calculations are often performed using density functional theory (DFT), which is applied to describe micro- and mesoporous carbon materials [28].

There are two types of plots commonly used to represent the pore size distribution of activated carbon: the $dS/dlog(D)$ vs. D plot, which is typically used to evaluate the contribution of pores of any size to the specific surface area, and the $dV/dlog(D)$ vs. D plot, which is more convenient for comparing the relative pore volumes according to the pore size distribution [29, 30]. In this study, the obtained pore size distribution indicates that all samples predominantly possess a microporous structure with a noticeable contribution of mesopores, which decreases with increasing activation temperature. The $dV/dlog(D)$ vs. D plot obtained via DFT analysis shows that the broad pore distribution (0.5–30 nm) of the seven activated carbon samples is primarily determined by two maxima at pore diameters of 0.5–2 nm and 5–7 nm (Fig. 5). On the other hand, the $dS/dlog(D)$ vs. D plot indicates that the specific surface area of the synthesized activated carbons is mainly provided by pores up to 10 nm in size, with the contribution of macropores being negligible.

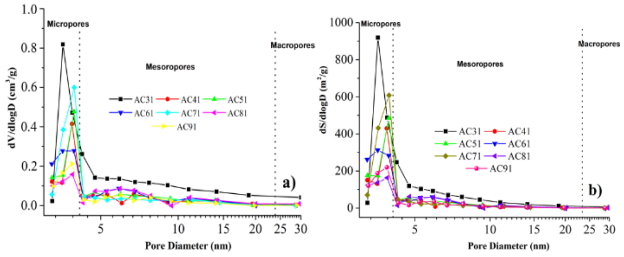

Fig. 5 – Pore size distribution curves of activated carbon samples obtained at different carbonization temperatures: (a) differential pore volume (dV/dlogD) and (b) differential pore surface area (dS/dlogD)

However, the histograms of the dependence of the specific surface area (SSA) on pore diameter (Fig. 6) show that the surface area is determined primarily by the contribution of pores significantly smaller than 10 nm, which differs markedly from the results obtained by DFT measurements. All activated carbons are characterized by a microporous structure with an average pore size of 0.5–1.5 nm. Among the synthesized materials, AC31 stands out, for which a significant contribution of mesopores with diameters of 3–4 nm is clearly observed. These conclusions are further supported by the values of the specific surface area of activated carbons carbonized at different temperatures, calculated based on adsorption isotherm analysis using BET and DFT theories (Table 2).

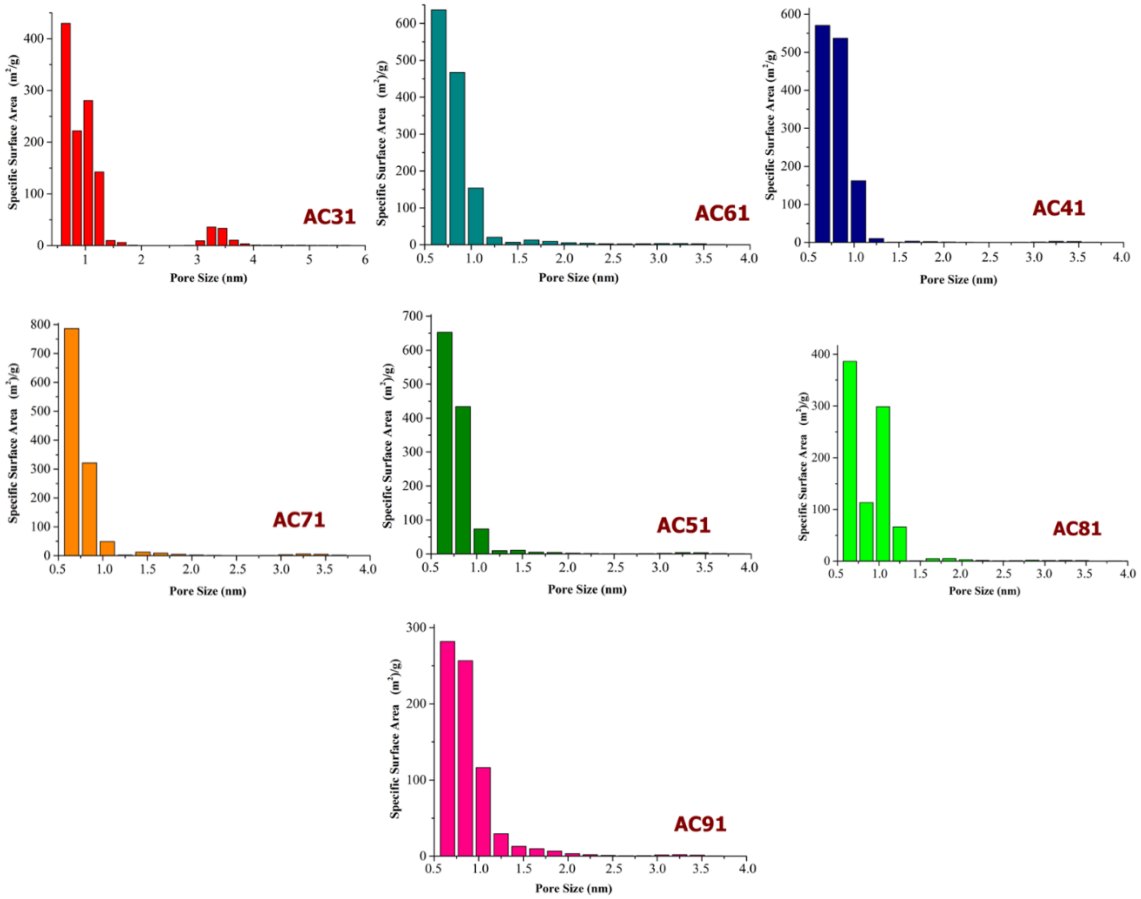

Fig. 6 – Histograms comparing the specific surface area of activated carbons obtained at different carbonization temperatures with the pore size

Table 2 – Micropore volume values of synthesized activated carbons obtained by different methods

Sample	AC31	AC41	AC51	AC61	AC71	AC81	AC91
SBET, $m^2 \cdot g^{-1}$	1313	1188	1068	1213	1042	837	721
SDFT, $m^2 \cdot g^{-1}$	1196	1303	1216	1332	1214	894	731

The difference in specific surface area values may be associated with discrepancies between these two methods, since the BET method is based on the assumption that adsorption occurs layer by layer on macropores and mesopores and does not account for the volumetric filling of micropores, whereas DFT is based on the physical–mathematical modeling of pore filling of various sizes and takes into account the shape, size, and contribution of micropores to the total porosity [31]. Consequently, in micro- and mesoporous carbon materials, DFT always indicates a higher specific surface area.

To determine the surface area of mesopores and the pore size distribution, whose adsorption mechanism is described by the theory of capillary condensation, it is most appropriate to apply the Barrett–Joyner–Halenda (BJH) method [7, 32]. The pore size distribution is typically determined from the desorption isotherm, as it corresponds to a lower relative pressure for the same gas volume, i.e., less energy is involved. Thus, the desorption isotherm is closer to true thermodynamic equilibrium.

As mentioned earlier, for microporous materials in the presence of mesopores, the dependence of the

adsorbed gas volume V on t forms a straight line (Fig. 3), the extrapolation of which to the intersection with the V-axis allows for the determination of micropore volume, while the slope of the line is used to calculate the mesopore surface area. The calculation of mesopore sizes can be carried out using the Kelvin equation for cylindrical pores:

$$r_m = \frac{2\gamma V_L}{RT\ln(P/P_0)}, \quad (4)$$

where γ is the surface tension of nitrogen at its boiling point ($8.85 \cdot 10^7$ J·cm^{-3} at 77 K), V_L is the molar volume of liquid nitrogen (34.7 cm^3·mol^{-1}), T is the boiling temperature of nitrogen (77 K), P/P_0 is the relative nitrogen pressure, R is the molar gas constant, and r_m is the pore radius according to Kelvin [34]. However, since adsorption occurs on the pore walls prior to condensation, does r_m not represent the true pore radius, especially because the adsorbed layer remains on the walls during desorption. The true pore radius is calculated according to the equation $r_p = r_m + t$, where t is the thickness of the adsorbed layer. The statistical value of t is taken as 3.54 (V_{ads}/V_m), where 3.54 Å is the thickness of a molecular layer of nitrogen, and V_{ads}/V_m is the ratio of the adsorbed nitrogen volume at a given relative pressure to the volume required to form a complete monolayer on a nonporous sample of the same composition.

The statistical layer thickness was also estimated using the Halsey empirical equation [35]:

$$t_H\left[\mathring{\text{A}}\right] = 3.54 \cdot \left(\frac{5}{-2.303\log(P/P_0)}\right)^{1/3} \quad (5)$$

The values of the mesopore surface area calculated using the BJH method and the average pore diameter of activated carbons carbonized at different temperatures are shown in Fig. 7. The different development of the mesoporous structure of AC at various carbonization temperatures is related to chemical reactions and the surface texture of carbon. According to the curve, activated carbon AC31, carbonized at 300°C, exhibits the highest mesopore surface area (246 m^2·g^{-1}), provided by pores with an average diameter of 2.25 nm. Increasing the carbonization temperature to 400°C slows the development of mesoporosity (pore diameter 1.75 nm) and reduces the mesopore surface area by 85 %. At temperatures of 500–700 °C, the mesostructure changes more uniformly, with mesopore surface areas of 55–60 m^2·g^{-1}. Since the carbonization temperature range is relatively high (700–900°C), the volatile content in the biomass rapidly evaporates [36, 37]. Due to the limited content of volatiles in the raw material, this growth trend gradually slows with further temperature increases up to 900°C, resulting in a reduction in the mesopore fraction in the AC structure. Across the entire temperature range (400–900°C), a trend of pore diameter stability around 1.75–1.80 nm was observed, while for sample AC71, the pore diameter was slightly higher, reaching 1.85 nm.

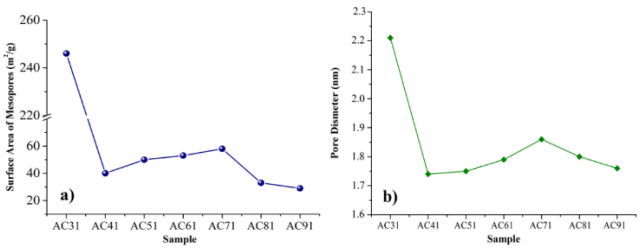

Fig. 7 – Surface area of mesopores(a) and pore diameter (b) of activated carbons obtained at different carbonization temperatures

Table 3 presents the details of the preparation of porous carbon materials reported in previously published studies, along with the results of the present work (arranged according to the treatment temperature). A comparison with recent literature data indicates that the pore structure and electrochemical performance of biomass-derived activated carbons are strongly governed by the combined effect of activation temperature and KOH impregnation ratio. Nowicki et al. used cherry pits as a precursor for the production of activated carbon [38]. It was found that changing the pyrolysis temperature (500 and 800 °C) followed by physical activation with CO_2 does not improve the surface porosity of the material, and the specific surface area (~367 m^2·g^{-1}) is provided mainly by micropores. Studies employing higher KOH-to-carbon ratios often report increased mesoporosity and surface area, but at the cost of reduced structural stability and higher carbon burn-off. Al-Ghurabi et al. employed date palm seeds as a precursor for carbon sorbents [39]. Among the series of samples, the optimal conditions for obtaining activated carbon with exceptional CO_2 adsorption capacity were determined to be 700 °C, 1.5 h, and an impregnation ratio of 3:1. However, the predominance of ultramicropores in the AC structure limits its practical application. Li et al. used an environmentally friendly organic activator on the surface of carbon materials via an in situ organic fermentation method [40]. The resulting AC exhibited a high S_{BET} value of 1354 m^2·g^{-1}; however, its practical use is limited due to the complexity of the three-stage synthesis process.

The type of precursor plays an important role in obtaining high-quality activated carbon with predetermined porous properties. For instance, Ahiduzzaman et al. investigated the production of AC from rice husk [41]. Since rice husk contains a high amount of silica, which hinders porosity, additional high-temperature treatment in an inert atmosphere is required to remove it from the structure. The resulting carbon material, despite having a relatively large pore size (~2.2 nm), is characterized by a complex synthesis process. In contrast, moderate ratios, comparable to those used in the present work, favor the development of stable microporous networks.

Table 3 – Characteristics of the porous structure of activated carbons obtained by thermal activation

Raw material of plant origin	Carbonization temperature, °C	Activation mechanism / conditions and agent-to-carbon weight ratio	Total pore volume, $cm^3 \cdot g^{-1}$	Specific surface area S_{BET}, $m^2 \cdot g^{-1}$	Average pore diameter, nm	Refs.
Cherry stones	500, 800	Physical/ CO_2 flow	0.190	~367	2-35–2.44	[38]
Date seed	700	Chemical/ KOH impregnation (3:1)	0.610	1502	>1.00	[39]
Biochar (general review)	700–900	Chemical/ KOH in situ organic fermentation treatment	0.500–0.850	~ 672–>1360	Predominantly microporous	[40]
Rice husk	700	Chemical/ $ZnCl_2$, impregnation (3:1)	0.160–0.880	331–645	~ 2.20	[41]
Sawdust from the trees	~ 700	Chemical/ KOH, one-step activation (2:1, 4:1)	0.315–0.400	672–912	> 1.00	[42]
Apricot pits	400–450	Chemical/ KOH-HNO_3, one-step activation (1:1)	0.521	1188	1.97	[43]
Phyllostachys edulis (bamboo)	700	Chemical/ KOH, one-step activation (1:1)	0.209	434	Not specified	[44]
Coconut husk	700	Physical/ steam and N_2 atmosphere	0.383	469	1.20	[20]
Apricot kernel shells (AC31)	300	Chemical/ KOH+water treatment (1:1)	0.684	1313	2.21	[This work]

Jedynak and Charmas, as in the present study, used KOH as an activator for producing AC from lignocellulosic biomass, specifically wood sawdust [42]. Compared to this work, the obtained activated biocarbon exhibited a well-developed microporous structure, with micropores contributing 85–97 % of the total pore volume depending on the precursor type.

Based on the obtained results, a two-stage process for producing activated carbon from apricot kernel shells, namely carbonization at 300°C followed by isothermal treatment of the pre-activated KOH–carbon at 900°C for 20 min, was identified as the optimal procedure for obtaining carbon material with a well-developed mesoporous structure.

4. CONCLUSIONS

Seven activated carbon (AC) materials were obtained by carbonization of apricot kernel shells followed by two-stage activation with potassium hydroxide at 900–920°C in an argon atmosphere. Their pore size distributions and porous structure parameters were analyzed using nitrogen adsorption isotherms at 77 K. All ACs exhibited type IV nitrogen adsorption–desorption isotherms, characteristic of mesoporous adsorption (> 2 nm).

The preparation temperature significantly influenced the pore size distribution, with micropores (< 2 nm) contributing predominantly to the total surface area. AC31, in particular, showed a large hysteresis loop, indicating a substantial contribution of mesopores. DFT analysis revealed pore size maxima in the ranges of 0.5–2 nm and 5–7 nm, with pore diameters decreasing as carbonization temperature increased.

A two-stage process–carbonization at 300 °C followed by isothermal treatment of KOH-activated carbon at 900°C for 20 min – was found optimal for producing carbon with a well-developed mesoporous structure. Under these conditions, the AC exhibited a specific surface area of 1313 $m^2 \cdot g^{-1}$ and a total pore volume of 0.680 $cm^3 \cdot g^{-1}$. Increasing carbonization temperature increased the micropore fraction, while the average pore diameter remained stable around 1.75–1.80 nm for all samples above 500°C. The maximum micropore volume, determined by the *t*-method, was observed for AC61 (0.469 $cm^3 \cdot g^{-1}$).

All the studies described above have both scientific and practical value. The identified features of the porous structure of apricot kernel shells allow for the establishment of optimal conditions for producing activated carbon through mechanical, chemical, and thermal treatments. The results indicate that the obtained activated carbon samples are comparable in their structural and adsorption properties to global analogues.

REFERENCES

1. W.K. Pui, R. Yusoff, M.K. Aroua, *Rev. Chem. Eng.* **35** No 5, 649 (2019).
2. J.M. Dias, M.C.M. Alvim-Ferraz, M.F. Almeida, J. Rivera-Utrilla, M. Sánchez-Polo, *J. Environ. Manag.* **85** No 4, 833 (2007).
3. V. Vashchynskyi, *Fuller. Nanotub. Carbon Nanostructures* (2025).
4. P. Branton, R.H. Bradley, *Adsorption* **17** No 2, 293 (2010).
5. A. Zabaniotou, G. Stavropoulos, V. Skoulou, *Bioresour. Technol.* **99** No 2, 320 (2008).
6. P. Paraskeva, D. Kalderis, E. Diamadopoulos, *J. Chem. Technol. Biotechnol.* **83** No 5, 581 (2008).
7. E.P. Barrett, L.G. Joyner, P.P. Halenda, *J. Am. Chem. Soc.* **73** No 1, 373 (1951).

8. K.S.W. Sing, *Pure Appl. Chem*. **57** No 4, 603 (1985).
9. A.M.M. Dubinin, Q. Rev., *Chem. Soc.* **9** No 2, 101 (1955).
10. J. Landers, G.Y. Gor, A.V. Neimark, *Colloids Surf. A Physicochem. Eng. Asp.* **437**, 3 (2013).
11. K.S.W. Sing, *Adv. Colloid Interface Sci.* **76-77**, 3 (1998).
12. V.M. Vashchynskyi, A.M. Boychuk, Y.B. Vashchynska, *J. Nano- Electron. Phys.* **11** No 3, 03012 (2019).
13. A. Swiatkowski, M. Pakula, S. Biniak, M. Walczyk, *Carbon* **42** No 15, 3057 (2004).
14. S. Brunauer, P.H. Emmett, E. Teller, *J. Am. Chem. Soc.* **60** No 2, 309 (1938).
15. M.M. Rahman, M. Muttakin, A. Pal, A.Z. Shafiullah, B.B. Saha, *Energies* **12** No 23, 4565 (2019).
16. X. Song, Y. Zhang, C. Yan, W. Jiang, C. Chang, *J. Colloid Interface Sci.* **389** No 1, 213 (2013).
17. N. Gibson, P. Kuchenbecker, K. Rasmussen, V.-D. Hodoroaba, H. Rauscher, *Characterization of Nanoparticles* (2020).
18. J.P.R.B. Walton, N. Quirke, *Mol. Simul.* **2** No 4-6, 361 (1989).
19. P.W.M. Jacobs, F.C. Tompkins, Q. Rev., *Chem. Soc.* **6** No 3, 238 (1952).
20. J. Fu, J. Zhang, C. Jin, Z. Wang, T. Wang, X. Cheng, C. Ma, *Bioresour. Technol.* **310**, 123413 (2020).
21. T. Boichuk, A. Boichuk, M.E. Changarath, M. Krečmarová, R. Abargues, V. Vashchynskyi, S. Agouram, J.F. Sánchez-Royo, *J. Power Sources* **655**, 237935 (2025).
22. H. Kurig, M. Russina, I. Tallo, M. Siebenbürger, T. Romann, E. Lust, *Carbon* **100**, 617 (2016).
23. D.F. Caulfield, *Fibre-Water Interactions in Paper-Making* (Fundamental Research Committee (FRC): Manchester: 1977).
24. A. Stein, Z. Wang, M.A. Fierke, *Adv. Mater.* **21** No 3, 265 (2009).
25. R.J. Dombrowski, C.M. Lastoskie, D.R. Hyduke, *Colloids Surf. A Physicochem. Eng. Asp.* **187-188**, 23 (2001).
26. A. Saito, H.C. Foley, *AIChE Journal* **37** No 3, 429 (1991).
27. A.V. Neimark, Y. Lin, P.I. Ravikovitch, M. Thommes, *Carbon* **47** No 7, 1617 (2009).
28. S.G. Chen, R.T. Yang, *Langmuir* **10** No 11, 4244 (1994).
29. R. Evans, U.M.B. Marconi, P. Tarazona, *J. Chem. Soc., Faraday Trans.* **2 82** No 10, 1763 (1986).
30. W. Zeng, G. Zhou, T. Cao, Z. Song, *Interpretation* **9** No 1, T21 (2021).
31. H. Tian, L. Pan, X. Xiao, R.W.T. Wilkins, Z. Meng, B. Huang, *Mar. Pet. Geol.* **48**, 8 (2013).
32. R. Bardestani, G.S. Patience, S. Kaliaguine, *Can. J. Chem. Eng.* **97** No 11, 2781 (2019).
33. V.M. Vashchynskyi, *Fuller. Nanotub. Carbon Nanostructures* **32** No 8, 747 (2024).
34. E. Lundquist, G. Parker, Jr. Rohm, *Proceedings of the 14th International Seminar on Double Layer Capacitors and Similar Energy Storage Devices* **14** No 69 (Deerfield Beach, FL, USA: 2004).
35. J.H. de Boer, B.C. Lippens, B.G. Linsen, J.C.P. Broekhoff, A. van den Heuvel, T.J. Osinga, *J. Colloid Interface Sci.* **21** No 4, 405 (1966).
36. M.S. Celiktas, F.M. Alptekin, *Energy* **188**, 116089 (2019).
37. V.M. Vashchynskyi, I.V. Semkiv, *Biofuels* **15** No 10, 1295 (2024).
38. P. Nowicki, J. Kazmierczak, R. Pietrzak, *Powder Technol.* **269**, 312 (2015).
39. E.H. Al-Ghurabi, M.M. Boumaza, W. Al-Masry, M. Asif, *Sci. Rep.* **15** No 1, 17132 (2025).
40. Y. Li, X. Yan, Z. Cui, J. Yuan, B. Xu, G. Yang, *Adv. Mater. Interfaces* **12** No 3, 2400450 (2024).
41. M. Ahiduzzaman, A.K.M. Sadrul Islam, *SpringerPlus* **5** No 1 1248 (2016).
42. K. Jedynak, B. Charmas, *Adsorption* **30**, 167 (2024).
43. V. Vashchynskyi, O. Okhay, T. Boychuk, *C* **9** No 4, 93 (2023).
44. Y. Guo, Q. Wang, *Processes* **10** No 9, 1712 (2022).

Дослідження розподілу пор в активованому вуглеці методом низькотемпературної адсорбції азоту

В.М. Ващинський, Я.Б. Ващинська

Національний університет «Львівська політехніка», 79013 Львів, Україна

Зразки активованого вуглецю (АВ) виготовлені з шкарлупи абрикосових кісточок за допомогою двостадійного процесу піролітичної активації. Було досліджено вплив температури карбонізації на пористу структуру та розподіл пор АВ. Результати показали, що висока температура та хімічна активація гідроксидом калію (КОН) стимулюють розвиток пористості. У цій роботі для аналізу структури пор використано метод фізичної адсорбції–десорбції азоту при 77 К в широкому діапазоні відносного тиску $P/P_0 = 0{,}050 – 1{,}0$. Карбонізація абрикосової шкарлупи при 300 °С прискорює випаровування летких речовин і призводить до появи більшої кількості мезопор, в той час як збільшення температури до 400 – 600°С сприяє розвитку мікропористої структури. Найбільша питома площа поверхні, визначена методом Брунауера-Еммета-Теллера (BET) отримана для зразка АС31 і становить 1313 м^2/г, а діаметр пор, визначений методом Барретта–Джойнера–Халенди (BJH) становив 2,25 нм. Значення V_{micro}, отримані для всієї групи синтезованих зразків АВ задовільно корелюють із значеннями, отримані методами Хорват–Кавазое (НК) та Сайто-Фолі (SF), що враховують вклад вузьких пор циліндричної форми. Згідно *t*-методу найбільший об'єм мікропор становить 0,469 см^3/г для зразка АС61, карбонізованого при 600 °С.

Ключові слова: Шкарлупа абрикосових кісточок, Температура карбонізації, Активований вуглець, Ізотерма адсорбції, Пориста структура.